Journal of Applied Electrochemistry **30**: 85–93, 2000.

Dynamic simulation of a parallel-plate electrochemical fluorination reactor

K. JHA[1], G.L. BAUER[2] and J.W. WEIDNER[1]*
[1]*Center for Electrochemical Engineering, Department of Chemical Engineering, University of South Carolina, Columbia SC 29208, USA;*
[2]*3M Chemicals, St. Paul MN 55144-1000, USA*
*(*author for correspondence)*

Received 2 July 1998; accepted in revised form 29 June 1999

Key words: fluorination reactor, time-dependent modelling

Abstract

A time-dependent mathematical model of a parallel-plate reactor was developed to study the electrochemical fluorination of organic compounds dissolved in anhydrous hydrogen fluoride. The model incorporates two-phase flow with differential material, energy and pressure balances. Dynamic results are presented that show the effect of disturbances to the whole reactor or one of the cells of the multicell reactor. The effect of disturbances in the cell current and inlet electrolyte flow rate on the cell voltage, molar flow rates, and current efficiency is studied. Also, the effect of a blockage in inlet flow to one cell in the cell pack is studied for cases when heat transfer is either present and absent between the adjoining cells.

List of symbols

A_{flow}	cross-sectional area for flow (cm^2)
d	separation gap between the plates in the cell pack (cm)
D	hydraulic diameter, $4A_{\text{flow}}/S_{\text{flow}}$ (cm)
f'	frictional factor multiplier
F	Faradaic constant (96 500 C equiv^{-1})
g	gravitational acceleration (981 cm s^{-2})
h	heat-transfer coefficient of electrolyte film (W cm^{-2} $^\circ\text{C}^{-1}$)
$\hat{H}$	average molar enthalpy of the two-phase mixture (J mol^{-1})
$\hat{H}_{\text{l}}$	liquid molar enthalpy (J mol^{-1})
$\hat{H}_{\text{v}}$	vapour molar enthalpy (J mol^{-1})
$\hat{H}_i$	molar enthalpy of species, i (J mol^{-1})
$\hat{H}_{i,\text{v}}$	molar enthalpy of species, i, in vapour phase (J mol^{-1})
$\Delta\hat{H}_{\text{r}}$	heat of reaction (J mol^{-1})
i	local current density (A cm^{-2})
$i_{\text{H}_2,\text{a}}$	hydrogen oxidation current (A cm^{-2})
k_{HF}	thermal conductivity of anhydrous liquid hydrogen fluoride (W cm^{-1} $^\circ\text{C}^{-1}$)
k_{Ni}	thermal conductivity of nickel electrode plate (W cm^{-1} $^\circ\text{C}^{-1}$)
L	length of each electrode in the cell pack (cm)
n	number of electrons taking part in hydrogen evolution reaction
$\dot{N}$	superficial molar flux of the two-phase mixture (mol cm^{-2} s^{-1})
$\dot{N}_{\text{H}_2}$	superficial molar flux of hydrogen in vapour phase (mol cm^{-2} s^{-1})
Nu	Nusselt number
P	total pressure (Pa)
Pr	Prandtl number ($\mu C_{\text{p}}/k_{\text{HF}}$)
$\dot{q}$	heat-transfer rate (W cm^{-3})
R	gas constant (8.314 J mol^{-1} K^{-1})
Re	Reynolds number ($\rho_{\text{l}} v_{\text{l}} D/\mu$)
S_{flow}	perimeter wetted by flow (cm)
t	time (s)
T	temperature (K)
$\hat{U}$	average internal energy of the two-phase mixture (J mol^{-1})
$\hat{U}_{\text{v}}$	molar internal energy of vapour (J mol^{-1})
$\hat{U}_i$	molar internal energy of species, i (J mol^{-1})
$\hat{U}_{i,\text{v}}$	molar internal energy of species, i, in vapour phase (J mol^{-1})
U_{h}	overall heat-transfer coefficient at electrode plate (W cm^{-2} $^\circ\text{C}^{-1}$)
v	average flow velocity of the two-phase mixture (cm s^{-1})
v_{m}	local mass-average velocity of the two-phase mixture (cm s^{-1})
$\bar{v}_{\text{m}}$	overall mass-average velocity of the two-phase mixture (cm s^{-1})
$\hat{V}_i$	molar volume of species i (cm^3 mol^{-1})
w	width of the planar electrodes in the cell pack (cm)
$\dot{w}_{\text{e}}$	input electrical power density (W cm^{-3})
x_{l}	molar flux of liquid per molar flux of two-phase mixture ($\dot{N}_{\text{l}}/\dot{N}$)
x_{v}	molar flux of vapour per molar flux of two-phase mixture ($\dot{N}_{\text{v}}/\dot{N}$)
y_i	mole fraction of species i in vapour phase
z	axial distance in the reactor (cm)

Greek symbols

β_v	volumetric flow rate fraction of vapour
κ	effective conductivity of the electrolyte (Ω^{-1} cm^{-1})
κ°	conductivity of bubble-free electrolyte (Ω^{-1} cm^{-1})
λ	thickness of electrode plate (cm)
μ	viscosity of the electrolyte (cP)
θ_v	volume fraction of vapour
ρ_{ave}	mass density of the two-phase mixture (g cm^{-3})
ρ'_{ave}	mass density of the two-phase mixture given by Equation 20 (g cm^{-3})
ρ_l	mass density of the liquid phase (g cm^{-3})
ρ_v	mass density of the vapour phase (g cm^{-3})
ρ_m	molar density of the two-phase mixture (mol cm^{-3})
$\rho_{m,l}$	molar density of the liquid phase (mol cm^{-3})
$\rho_{m,v}$	molar density of the vapour phase (mol cm^{-3})
σ	surface tension of the electrolyte (dyn cm^{-1})
$\dot{\xi}$	reaction rate (mol s^{-1})
τ	mass average residence time (s)

Subscripts

adj	adjacent cell
ave	average
drift	drift velocity
final	steady-state after disturbance
HF	oligomerized HF
H_2	hydrogen
initial	steady-state before disturbance
l	liquid
ref	reference state
RF	fluorochemical product
v	vapour

1. Introduction

Recently, a forced convective, bipolar flow reactor [1] has been developed as a replacement to the Simons cell [2] for the electrochemical fluorination of organic compounds. Although this new design reduces energy costs and increases production rates, a better understanding of the process is needed to minimize operational problems and maximize production rates. A time-dependent model of the reactor is developed in this work and used to study the effect of disturbances on the behaviour of the reactor and improve the understanding of the reactor operation.

This work is an extension of the previous steady-state models of an electrochemical fluorination reactor [3, 4]. These model results revealed that the fluorination reaction has operating characteristics not seen in other electrochemical reactors. For example, because the parasitic reaction (i.e., H_2 oxidation) involves a gaseous product, and the system operates at relatively high temperatures, the current efficiency in the fluorochemical reactor increases with cell current [3]. Higher currents result in higher temperature, which increases evaporation of the HF and lowers the partial pressure of H_2. This is in contrast to recent models of more typical systems where the rate of the parasitic reaction (i.e., H_2 evolution) increases with current [5, 7].

Therefore, due to this flow reactor's unique performance, we develop in this work a dynamic model of the electrochemical fluorination reactor. The model is then used to study two types of disturbances that can affect the controllability of the process. First, the effect of disturbances in cell current and flow rate on the voltage, efficiency and molar flow rates in the reactor are studied. The magnitude and time constant for the responses to disturbances provides insight into the dynamic response of the reactor. Second, the response of the reactor to blocking of the inlet flow distributor in one cell of the cell pack is studied with and without heat transfer between the cells.

2. Model development

2.1. *Description of the fluorination reactor*

The fluorination reactor (Figure 1) is comprised of five sections: (1) inlet pipe, (2) inlet flow-distributors, (3) cell pack, (4) outlet flow-distributors and (5) outlet pipe. The cell pack consists of 26 identical parallel-plate cells and each cell has 18 inlet and outlet flow distributors. The flow distributors are narrow channels evenly placed along the width of each cell, providing uniform flow to all the cells in the cell pack under normal operation.

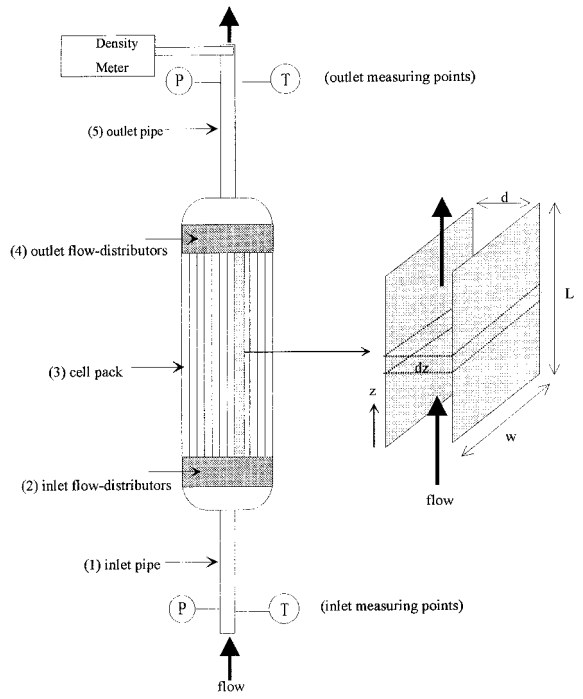

Fig. 1. Schematic of the electrochemical fluorination reactor. Inlet and outlet measurement points for temperature, pressure and density are indicated. A magnified view of one of the parallel-plate cells is also shown.

Hydrogen evolution occurs at the cathode, and the following two reactions occur at the anode:

$$RH + 2F^- \rightarrow RF + HF + 2e^- \quad (A)$$

$$H_2 \rightarrow 2H^+ + 2e^- \quad (B)$$

where RF is the fluorinated organic compound, HF is anhydrous liquid hydrogen fluoride and RH is the fluorinatable organic compound. The electrochemical fluorination reaction at the anode is catalysed by complex nickel fluorides present in a thin anodic film. Due to the use of an undivided cell, some of the hydrogen produced at the cathode is transported to, and oxidized at the anode. Therefore, the current efficiency of the electrochemical fluorination is less than unity. The overall reaction for the fluorination process can be represented as

$$RH + HF \rightarrow RF + H_2 \quad (C)$$

2.2. *Assumptions*

The assumptions used to model the electrochemical fluorination process are identical to those used in the previous work [3] except for the relaxation of the following three assumptions:

(i) The vapour and liquid velocities are not necessarily equal (i.e., the no-slip criteria between the two phases has been relaxed).
(ii) All the 26 parallel-plate cells in the reactor may not behave identically. A disturbance can be applied to just one cell out of the 26 cells (e.g., partial blockage of its flow distributors).
(iii) Heat transfer can occur between plates in the cell pack of the reactor.

2.3. *Governing equations*

The governing equations are identical to those used in the steady-state model [3] except for the time dependent material and energy balances, and changes arising from the additional assumptions noted above. Therefore, only the balances and equations that differ from the steady-state model are presented here.

2.3.1. *Molar balance*

The overall, steady-state molar balance given previously [3] is replaced by the following dynamic equation:

$$\frac{\partial \rho_m}{\partial t} = -\frac{\partial \dot{N}}{\partial z} \quad (1)$$

Equation 1 reflects the fact that there is no net change in moles in the overall reaction (Reaction C).

Similarly, an individual balance on hydrogen, which relates the accumulation of moles of hydrogen in the vapour phase to the gradient in the molar flux and the net production of hydrogen (i.e., generation of the cathode minus consumption at the anode), is given by

$$\frac{\partial (y_{H_2} x_v \rho_m)}{\partial t} = -\frac{\partial \dot{N}_{H_2}}{\partial z} + \frac{(i - i_{H_2,a})}{nFd} \quad (2)$$

The hydrogen oxidation current is assumed to be mass-transfer limited across the salt film on the anode [3].

2.3.2. *Energy balance*

An energy balance in each of the flow sections relates the rate of change of local internal energy to the change in energy due to electrolyte flow, the rate of electrical work done on the fluid, $\dot{w}_e$, the energy transferred from the surroundings, $\dot{q}$, and the energy consumed by the heat of reaction as follows:

$$\frac{\partial (\rho_m \hat{U})}{\partial t} = -\frac{\partial (\dot{N}\hat{H})}{\partial z} + \dot{w}_e + \dot{q} - \dot{\xi}\Delta H_r \quad (3)$$

The changes in the kinetic and potential energies along the reactor are negligible compared to enthalpy changes. The relationship between the average molar enthalpy of the two-phase stream ($\hat{H}$), and its temperature and phase was given previously [3].

For an incompressible liquid, the internal energy is the equal to its enthalpy. Therefore, the two-phase internal energy can be expressed as follows:

$$\hat{U} = x_v \hat{U}_v + x_l \hat{H}_l \quad (4)$$

where the internal energy of the vapour phase is given by

$$\hat{U}_v = y_{H_2} \hat{U}_{H_2} + y_{RF} \hat{U}_{RF,v} + y_{HF} \hat{U}_{HF,v} \quad (5)$$

The specific internal energy of each species, i, in the vapour phase is related to its specific enthalpy by the following equation:

$$\hat{U}_{i,v} = \hat{H}_{i,v} - (P\hat{V}_i - P_{ref}\hat{V}_{i,ref}) \quad (6)$$

The reference state of hydrogen is a gas at standard conditions. Assuming ideal gas law behaviour, Equation 6 for hydrogen can be written as

$$\hat{U}_{H_2} = \hat{H}_{H_2} - R(T - T_{ref}) \quad (7)$$

For HF and RF, the reference state is liquid at standard conditions. The liquid specific volume is assumed to be much lower than the specific volume in the vapour state. Combining this assumption with the ideal gas law, Equation 6 for RF and HF is

$$\hat{U}_{i,v} = \hat{H}_{i,v} - RT \quad (8)$$

Substituting Equations 7 and 8 and an analogous expression to Equation 5 for $\hat{H}_v$ [3] into Equation 5

gives the specific internal energy of the vapour phase as follows:

$$\hat{U}_v = \hat{H}_v - y_{H_2} R(T - T_{ref}) - (y_{RF} + y_{HF})RT \quad (9)$$

Equation 9 is used in conjunction with Equation 4 to calculate the internal energy of the two-phase mixture.

As described previously [3], the electrical work done on the fluid in each cell depends on the effective conductivity of the electrolyte. The effective conductivity of the electrolyte is related to the pure electrolyte conductivity, κ°, and the volume fraction of the vapour phase, θ_v, by the Bruggeman equation as follows [8]:

$$\kappa = \kappa^\circ (1 - \theta_v)^{1.5} \quad (10)$$

The volume fraction of vapour, θ_v, is the volume occupied by the vapour per unit volume of the two-phase mixture at any position in the reactor. Previously [3] it was assumed that there is no slip between the vapour and liquid phases. Therefore, the volume fraction of vapour, θ_v, was identical to the volumetric flow fraction of vapour, β_v, which is the ratio of the volumetric flow rate of the vapour to the volumetric flow rate of the two-phase mixture. However, for the case of slip between the vapour and liquid phases, θ_v is lower than β_v, as the velocity of the vapour is more than that of the liquid phase. For narrow channels having a separation distance of 0.8–3.0 mm, the buoyancy effects can be neglected and θ_v can be related to β_v by the following equation [9]:

$$\theta_v = 0.8\,\beta_v \quad (11)$$

The above correlation is for an air–water system. It is expected that the lower surface tension of HF compared to water ($\sim$6 dyn cm^{-1} for HF and $\sim$70 dyn cm^{-1} for water) will result in less slipping of the vapour past the liquid [10]. However, given the lack of experimental data on hydrogen–HF system, the data from the air–water system can be used as an upper bound to the degree of slip occurring between the vapour and liquid for the hydrogen–HF system.

The volumetric flow fraction, β_v, is related to the molar flow fraction of the vapour, the partial molar density of the vapour, and the average molar density of the two-phase mixture by the following equation:

$$\beta_v = \frac{x_v \rho_m}{\rho_{m,v}} \quad (12)$$

Equations 11 and 12 are used to calculate the volume fraction of vapour in the cells of the cell pack and the inlet and outlet flow distributors. However, Equation 11 should not used for the outlet pipe as it has a diameter much greater than 3 mm. The distribution parameter theory [10–12] is used to calculate the volume fraction of vapour in the outlet pipe by the following equation:

$$\theta_v = \frac{v_v}{1.1\,v + v_{v,drift}} \quad (13)$$

where v_v is the superficial vapour velocity, v is the two-phase mixture velocity, and $v_{v,drift}$ is the drift velocity of the vapour. The vapour velocity is calculated as

$$v_v = \frac{\dot{N} x_v}{\rho_{m,v}} \quad (14)$$

The two-phase mixture velocity is the sum of the superficial velocities of the liquid and vapour phases and expressed as

$$v = \frac{\dot{N} x_v}{\rho_{m,v}} + \frac{\dot{N} x_l}{\rho_{m,l}} \quad (15)$$

In general, the vapour drift velocity, $v_{v,drift}$, used in Equation 13, is related to the two-phase flow regime and orientation, size of the vapour bubbles, and the surface tension, of the electrolyte, density and viscosity [10]. Although the bubble sizes are difficult to measure or predict, the turbulent flow present in the outlet pipe enable a reasonable estimate of the drift velocity without knowledge of the bubble size to be obtained [10, 12]:

$$v_{v,drift} = 3.28\left(\frac{\sigma g}{\rho_l}\right)^{0.25} \quad (16)$$

As stated in assumption (iii), the model used in the present study has the capability of having heat transfer between adjacent cells in the cell pack. The rate of energy exchange between a perturbed and adjacent cells is related to the heat transfer coefficient and the temperature difference as follows:

$$\dot{q} = \frac{2U_h(T - T_{adj})}{d} \quad (17)$$

where T and T_{adj} are the temperatures in the perturbed cell and the 25 adjacent cells, respectively. In reality, all 25 adjacent cells will not be at the same temperature. Rather, the temperature of the cells immediately adjacent to the perturbed cell will be between T and the temperature of the cells farther away. Using a higher T_{adj} in Equation 17 would result in a lower heat transfer rate between the cells. Therefore, the rate of heat transfer used in this study serves as an upper bound to the heat-transfer rate.

Assuming the heat-transfer resistance of the anodic film to be negligible, the overall heat-transfer coefficient at each plate in the perturbed cell is related to the liquid film heat-transfer coefficient on both sides of the plate, and the thermal conductivity and thickness of the nickel electrode plate by the following equation:

$$\frac{1}{U_h} = \frac{1}{h} + \frac{\lambda}{k_{Ni}} + \frac{1}{h_{adj}} \quad (18)$$

For turbulent flow, the liquid film heat-transfer coefficient is related to the Nusselt number, and subsequently to the Reynolds and Prandtl number by [13]:

$$h = \frac{Nu\, k_{HF}}{D} = 0.027\, Re^{0.8} Pr^{0.33} \left(\frac{k_{HF}}{D}\right) \tag{19}$$

The above correlation for turbulent flow is used here even though there may be regions of laminar flow present in the cell for some operating flow rates. Equation 19 gives values for the heat-transfer coefficient higher than that predicted by correlations for laminar flow. Again, the results shown with heat transfer can be considered an upper bound to the heat-transfer rate, and those without heat transfer as the lower bound.

2.3.3. *Pressure balances*

The pressure drop is composed of contributions from the elevation, frictional, and kinetic pressure drops. The equations for these pressure drops are the same as given previously [3], but some of the terms in these equations are different due to the removal of the no-slip assumption. For one, the velocity used in the calculations for the kinetic and frictional pressure drops is the mixture velocity, v, given by Equation 15. Also, in calculating the kinetic pressure drop, the two-phase density based on the volumetric flow rate fractions, ρ'_{ave}, should be used instead of that based on the volume fractions of the vapour and liquid phases, ρ_{ave} (see [3] for ρ_{ave} relationship). This is because the energy entering and leaving a differential element of the flow section is a function of the properties of the fluid entering and leaving the differential element, not of the fluid in the volume element [14]. The two-phase density, ρ'_{ave}, can be expressed as a function of the volumetric flow rate fraction of vapour, β_v, and the densities of the vapour and liquid phases by the following equation:

$$\rho'_{ave} = (1 - \beta_v)\rho_l + \beta_v \rho_v \tag{20}$$

When there is slip between the vapour and liquid, the friction factor multiplier, f', is calculated by the following equation obtained by fitting the predictions of Beggs and Brill [14] over the vapour volume fraction range of 0–1:

$$f' = 1.234 + 0.315 \ln\left(\frac{1 - \beta_v}{(1 - \theta_v)^2}\right) \tag{21}$$

Note that the above equation reduces to Equation 43 in the previous work [3] when the no-slip criteria is used (i.e., the volume fraction of vapour, θ_v is equal to volumetric flow fraction of vapour, β_v).

2.4. *Solution procedure*

The governing equations are applicable for each of the 26 parallel-plate cells in the cell-pack. All the equations were programmed using Speedup™ (Aspen Technology's equation-based dynamic flowsheet simulator software.) for three main advantages: (i) a choice of built-in time integrators and algebraic equation solvers; (ii) facility of linking the various reactor section models among each other and to models of other process units; and (iii) ability to link to Properties Plus™, Aspen Technology's physical-properties database. Implicit Euler's method with a step size of 0.05 second was used for the time integration and three-point finite-difference technique was used in the spatial direction. Two types of disturbances were simulated in this paper: (i) the same disturbances was applied to all the 26 cells; and (ii) a disturbances was applied to one of the 26 cells. Prior to both types of disturbances, the reactor was at steady state.

The model can be generalized to handle variations in and interactions among all the cells in the cell pack. However, for the results shown here, the interactions are restricted to the two cell sets (i.e., the perturbed cell, and the adjacent cells in the cell pack). The conditions within each cell set are identical. Two constraints are used in linking the cell sets to the flow system: (i) equality of pressure on either ends of the cells (i.e., before the inlet flow distributor and after the outlet flow distributor), and (ii) equality of the cumulative electrolyte flow in the cells to the flow in the inlet pipe. When a disturbance is applied to the perturbed cell, the adjacent cells are affected through heat transfer and flow redistribution. Allowing interaction among more than two sets of cells was performed, but the effects on the perturbed cell were insignificant for the results shown here. As stated earlier, the case with heat transfer can be treated as an upper bound to the effect of heat transfer on the responses to disturbances.

3. Results and discussion

The model was used to study the following two types of disturbances:

(i) The effect of a disturbance in inlet flow rate and current on voltage, efficiency, and molar flow rate.
(ii) The response of voltage, efficiency, and molar flow rate to the blocking of the inlet flow distributor in one cell of the cell pack. Responses were studied with and without heat-transfer interaction between the cells.

The values for the cell dimensions, physical parameters, and operating conditions that are common to all results shown here are either listed in Tables 1 and 2, or given in [3].

3.1. *Effect of a disturbance in the current and flow rate*

The effect of step changes in the cell current and feed flow rate on the outlet molar flow rates, cell voltage and the current efficiency of the reactor was studied. The other operating conditions (outlet pressure and inlet temperature) were kept constant at values shown in

Table 1. Physical parameters used in the simulations that are introduced due to the dynamic balances and changes arising from the additional assumptions given in Section 2.2. All other parameters used in the simulations can be found in [3]

Surface tension of HF, σ	6 dyn cm^{-1}
Thermal conductivity of nickel electrode, k_{Ni}	0.9 W cm^{-1} $°C^{-1}$
Thickness of nickel electrode, λ_{Ni}	0.2 cm
Thermal conductivity the HF electrolyte, k_{HF}	0.41 W cm^{-1} $°C^{-1}$

Table 2. For these studies, all the cells in the cell pack were assumed to behave identically before and after the disturbance was applied.

The effect of a step change in the cell current on the outlet molar flow rate, while holding the feed flow rate constant, is shown in Figure 2. This figure shows the responses of the outlet molar flow rate for two levels of initial current (350 and 700 A) and with a 5% and 10% increase in each cell current. Following a current disturbance at 2 s, the outlet molar flow rate experiences a steep rise when the disturbance is applied and then it gradually recovers to its original steady-state value. An increase in the cell current leads to higher power input and therefore, more evaporation and higher flow rate of the two-phase mixture. Eventually, the outlet molar flow rate approaches the value of inlet flow rate. The height of the peak in the outlet flow depends on the magnitude of the disturbance. For example, a 10% increase in the current produces a peak in the outlet flow rate that is 5% greater than the inlet flow rate, while a 5% disturbance produces a peak that is 2.5% greater than the inlet flow rate. For all four disturbance responses shown in Figure 2, the flow rate recovered 90% of its peak height in approximately 5 s after the application of the disturbance.

The four disturbances that caused the outlet flow rate to spike in Figure 2 had a less noticeable effect on the cell voltage and current efficiency. Both the cell voltage and current efficiency increased and stabilized at their new steady state very quickly when the step change in current was applied. For example, both these dependent variables reached approximately 90% of their final steady values within 1 s for the disturbance conditions associated with Figure 2. A fast response time was also observed for more severe disturbances.

The effect of a step change in the inlet flow rate, while holding the current constant, is shown in Figures 3, 4 and 5 for outlet molar flow rates, cell voltages, and current efficiencies, respectively. As with Figure 2, the disturbance was applied after the simulation was run at steady state for 2 s. Figure 3 shows the effect on the outlet flow rate to a 10% and a 20% decrease in the inlet flow rate. The response is shown for two initial inlet flows (5.0 and 2.5 l s^{-1}) at two currents (700 and 350 A). For comparison, the inlet flow rates are shown by the dotted lines. The outlet flow rate drops steeply in the beginning as the inlet flow is reduced. The initial drop in the flow rate is higher at 350 A compared to 700 A because at low currents, the two-phase mixture is predominantly liquid and the system is able to equilibrate more quickly. After the initial drop, the outlet flow rate reduces gradually due to evaporation of HF before dropping quickly again due to backpressure from the outlet flow distributors. The outlet flow rate drops slowly after the second steep drop until it matches the inlet flow rate. For a cell current of 700 A, the outlet flow rate achieves 90% of its steady-state value in 7.5 and 6 s following a 20% drop in the initial inlet flow rate of 2.5 and 5.0 l s^{-1}, respectively.

The effect of a step decrease in the inlet flow on the cell voltage and current efficiency are shown for a cell current of 700 A in Figures 4 and 5, respectively. The cell voltage rises slightly (~1%) due to a small rise in the

Table 2. Operating conditions used in obtaining simulation results presented in Figures 2–10

Inlet temperature	32 °C
Outlet pressure	2.0 atm

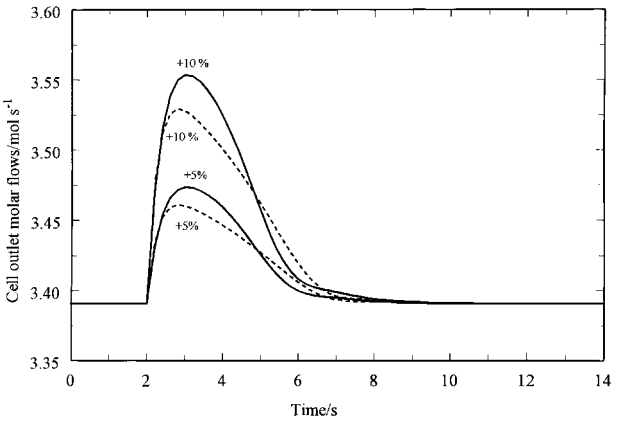

Fig. 2. Response of the molar flow rate at the outlet of a cell to a step change in cell current. Results are shown for 5 and 10% increases in cell current for initial currents of 350 (- - - -) and 700 A (——). Disturbance was applied at $t = 2$ s. Reactor feed flow rate was held constant at 5.0 l s^{-1}.

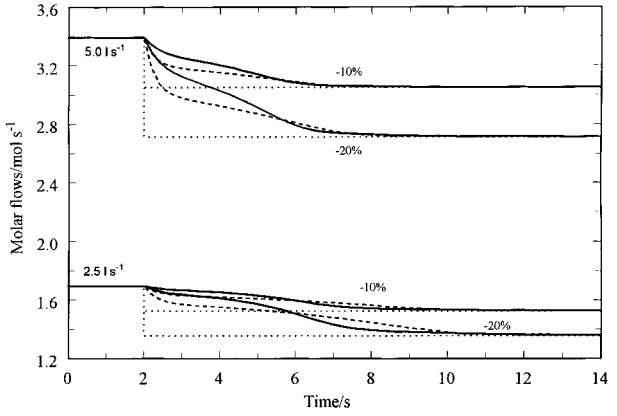

Fig. 3. Response of the outlet molar flow rate to a step change in inlet flow rate. Results are shown for 10 and 20% decreases in the inlet flow rate from 2.5 and 5.0 l s^{-1} for two cell currents, 350 (- - - -) and 700 A (——). Disturbance was applied at $t = 2$ s. Inlet flow: (· · · ·).

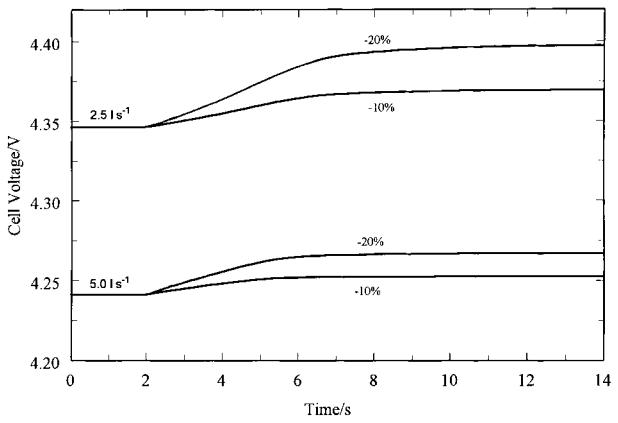

Fig. 4. Response of the cell voltage to a step change in the inlet flow rate. Results are shown for 10 and 20% decreases in the inlet flow rate from 2.5 and 5.0 l s^{-1} at a cell current of 700 A. Disturbance was applied at $t = 2$ s.

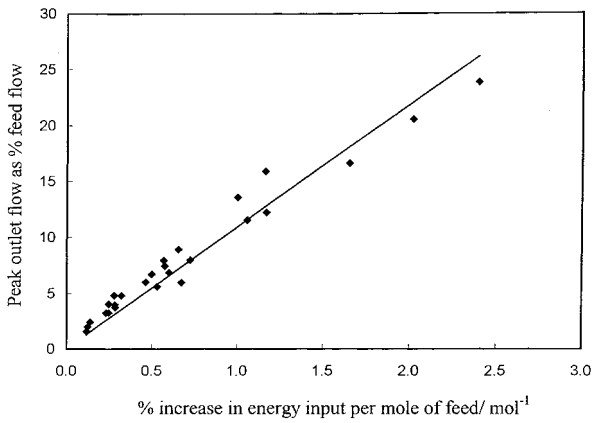

Fig. 6. Peak outlet flow rate as a function of energy input following a step change in the current. Simulation results and best fit line are represented by symbols and solid line, respectively.

cell's ohmic resistance. The rise is more for the lower flow rate (2.5 l s^{-1} compared to 5.0 l s^{-1}) because of a larger volume fraction of vapour at low flows. The current efficiency in Figure 5 also shows a small increase (~1%) when the flow rate is decreased. The evaporation of HF in the cell reduces the concentration of hydrogen, which decreases the hydrogen reoxidation current relative to the cell current. For a cell current of 700 A, the cell voltage achieved 90% of its steady-state value in 5.5 and 3.6 s following a 20% drop in the initial inlet flow rate of 2.5 and 5.0 l s^{-1}, respectively. For the same cell current and flow-rate changes, the current efficiency achieved 90% of its steady state value in 3.7 and 1.7 s, respectively.

Figures 2–5 illustrate the responses of the flow rate, cell voltage and current efficiency to disturbances in cell current and flow rate. However, only specific cases were shown in those Figures. The characteristics of these responses are summarized in Figures 6–8 for a wide range of flow rates (1.5–5.0 l s^{-1}) and cell currents (100–800 A) following a disturbance. The range of operating conditions cover the regions where the two-phase mixture is predominantly liquid to where it becomes predominantly vapour on a volumetric basis. In each Figure, a linear best fit line is shown along with the discrete simulation results represented by symbols. Figure 6 shows that when a step change in current is applied at constant inlet flow rate, the peak in the outlet molar flow rate as a percentage of the inlet flow is linearly dependent on the percentage change in energy input per mole of feed. This implies that the increase in the rate of evaporation of the electrolyte (resulting in the peak in the outlet flow rate) is directly related to the percentage in the energy input per mole of electrolyte feed.

Peaks were observed only in the response of the outlet molar flow rate to disturbances in current at a constant inlet flow rate. However, a characteristic of all the responses was the time taken for each variable to reach steady state after a disturbance was applied. The response time for each of the three variables (i.e., outlet molar flow rate, voltage, and current efficiency) is defined as the time it takes to reach 90% of their maximum difference between the initial and final steady-

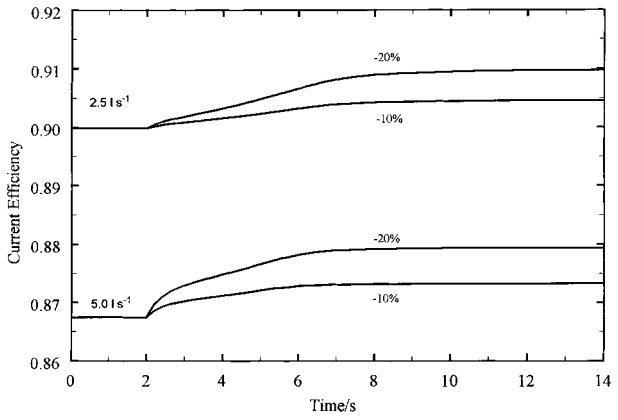

Fig. 5. Response of the current efficiency to a step change in the inlet flow rate. Results are shown for 10 and 20% decreases in the inlet flow rate from 2.5 and 5.0 l s^{-1} at a cell current of 700 A. Disturbance was applied at $t = 2$ s.

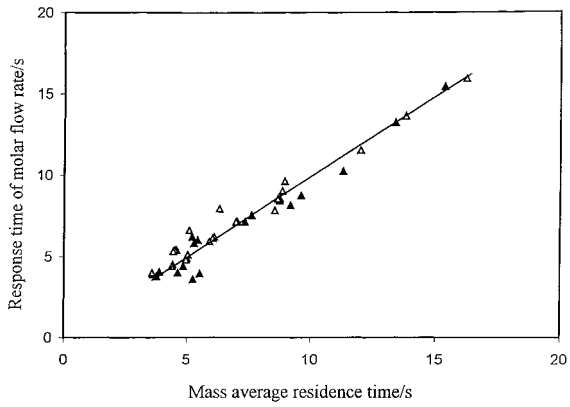

Fig. 7. Response time of outlet molar flow rate as a function of mass-average residence time in the cell. Simulation results and best fit line are represented by symbols and solid line, respectively. Step changes: (△) in current; (▲) in flow rate.

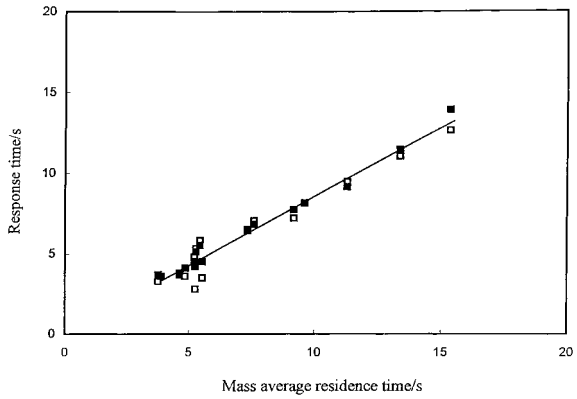

Fig. 8. Response time of cell voltage and current efficiency to mass-average residence time in the cell. Simulation results and best fit line are represented by symbols and solid line, respectively. Key: (□) current efficiency; (■) voltage.

state values. For example, to calculate the response time of the outlet molar flow rate, the magnitude of the peak in the flow rate is measured and it is used to find the time taken to recover 90% of the peak relative to steady state. The cell voltage and current efficiency do not show peaks and therefore, the response time of each of these variables is the time taken to approach 90% of their change between the initial and final steady state values.

Figures 7 and 8 show that the response time of the molar flow rate, voltage, and current efficiency increases linearly with the mass average residence time. The response times for the molar flow rates shown in Figure 7 are for case studies having step changes in cell current and feed flow rate. For the cell voltage and current efficiency, the response times are for step changes in the feed flow rate only. As stated earlier, a step change in the current resulted in very small response times for cell voltage and current efficiency.

A variety of residence times were correlated to the responses shown in Figures 7 and 8. The mass-average residence time correlated the best to the responses. This residence time is the time that a unit mass of the two-phase mixture stays in the cell pack. It combines the effects of the vapour volume fraction and the velocities of vapour and liquid phases at the initial and final steady states. To calculate this residence time, the local mass-average velocity of the two-phase mixture at each point in the cell pack was calculated by summing the contributions of the vapour and liquid phases.

$$v_{\mathrm{m}}\rho_{\mathrm{ave}} = \rho_{\mathrm{v}}v_{\mathrm{v}}\theta_{\mathrm{v}} + \rho_{\mathrm{l}}v_{\mathrm{l}}(1-\theta_{\mathrm{v}}) \tag{22}$$

Then the overall mass-average velocity was calculated by averaging the local mass-average velocity over the length of the cell pack

$$\bar{v}_{\mathrm{m}} = \frac{\int_0^L v_{\mathrm{m}}\mathrm{d}z}{L} \tag{23}$$

Finally, the mass-average residence time was calculated by dividing the length of the reactor by the values of the mass-average velocity at the steady states before and after the applied disturbance, as shown below:

$$\tau = \frac{L}{0.5(\bar{v}_{\mathrm{m,initial}} + \bar{v}_{\mathrm{m,final}})} \tag{24}$$

The strong correlation seen in Figures 7 and 8 between the system response time to a disturbance and the mass-average residence time provides a convenient means of predicting system instabilities *a priori*.

3.2. *Effect of blockage of flow distributors on the behaviour of a cell in the cell pack*

For the results shown in Figures 2–8, all the cells in the multicell cell pack were assumed to behave identically. However, it is possible that one cell or sets of cells may start behaving differently from the rest of the cell pack. One of the phenomena that may occur is a sudden or gradual blockage of the inlet flow distributors in one cell due to deposition of organic material. The effect of blocking of the flow distributors was studied and the results are presented in Figures 9 and 10. The simulations were performed for different currents and number of blocked flow channels. The number of channels available for flow was 18 initially. The results are shown for the cases of negligible heat transfer and appreciable heat transfer. Negligible heat transfer can occur when a set of cells gets disturbed and therefore the cell in the middle of the disturbed cell set has negligible heat transfer with the adjacent cells. Negligible heat transfer can also occur if the plates of the disturbed cell become fouled. In practical situations, the amount of heat transfer would be intermediate between the negligible and appreciable heat transfer used in this paper.

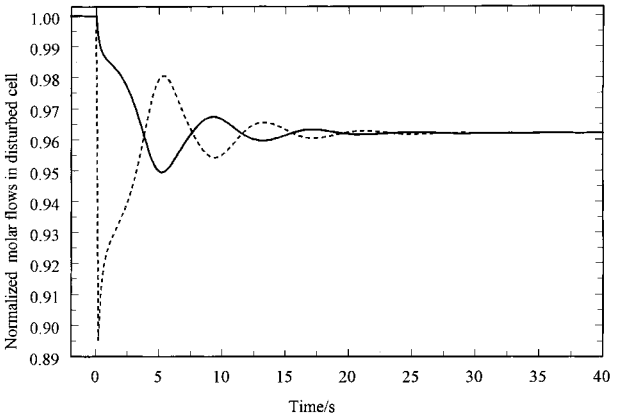

Fig. 9. Response of the inlet (- - - -) and outlet (——) molar flow rates in a perturbed cell to sudden blocking of the inlet flow distributors without heat transfer between the cells. Results shown are for a cell current of 700 A, an inlet flow rate of 2.5 l s^{-1}, and blocking of three out of 18 inlet flow distributors. Distributors were blocked at time equal to zero.

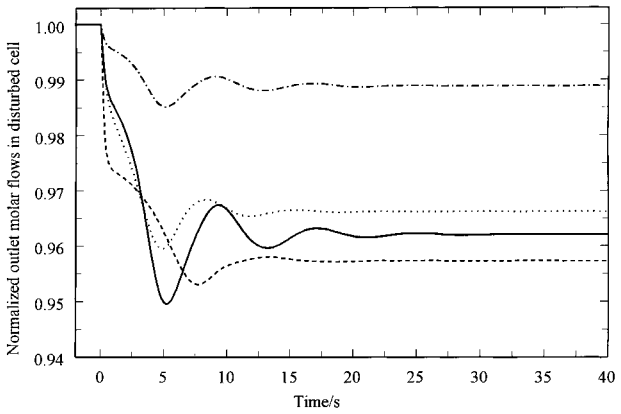

Fig. 10. Responses of the outlet molar flow in the perturbed cell to different magnitudes of blocking of the inlet flow distributors at different cell currents and with/without heat transfer between adjacent cells. Distributors were blocked at time equal to zero. Key: (–·–·–) 700 A, 1 blocked, no heat; (·····) 700 A, 3 blocked, with heat; (——) 700 A, 3 blocked, no heat; (- - - -) 350 A, 3 blocked, no heat.

Figure 9 shows the effect of blocking of 3 of the 18 inlet flow distributors at time equal to zero on the normalized inlet and outlet molar flow rates of the perturbed cell. The flow rates are normalized using the inlet flow rate prior to the disturbance. The results are for a cell current of 700 A and no heat transfer between the cells. Both the inlet and outlet flow rates are presented to show the typical response of the cell on blocking. The blocking of a flow distributor results in an immediate drop in the inlet flow rate. There is a corresponding drop in the outlet flow rate and then oscillations in both the inlet and outlet flow rate values until they become equal at the new steady state. The time periods of the oscillations remain approximately 7–8 s until a new steady state is reached.

The effect of blocking of the flow distributors for different values of cell current and blockage, with and without heat transfer, are shown in Figure 10. Comparing the cases for 350 A and 700 A for three blocked flow channels and without heat transfer, it can be seen that the oscillations are more pronounced at higher currents. The result for 350 A has one oscillation compared to multiple ones for 700 A. This is because the fluid in the cell is in a predominantly liquid phase at low currents and therefore more stable to changes in flow rate due to a large evaporative capacity. At higher currents, the instability is higher due to higher vapour volume fractions present, leading to more interactions with the operating temperatures and pressures. Comparing cases of 700 A without heat transfer and blocking of one and three flow channels, it can be seen that even though the magnitude of the oscillations is lower for one blocked cell, the oscillatory behaviour is almost identical. Comparison of cases at 700 A, three blocked channels, and with and without heat transfer, shows that the presence of heat transfer significantly dampens the oscillations besides resulting in a different steady state. Presence or absence of heat transfer determines the new steady-state temperatures and corresponding effects on the pressure and vapour volume fractions. Therefore, the final steady states for cases with and without heat transfer are different for the disturbed cell. The cell voltage and efficiency also experience oscillations similar to those shown for the molar flow rate in Figure 10. However, the maximum change in these variables is less than 0.5%.

4. Conclusions

A dynamic first principles model of a parallel-plate fluorination reactor was developed. The effects of disturbances in the cell current and in the inlet flow rate on the molar flow rates in the cell, the cell voltage and the current efficiency were studied. The response times of these variables was found to depend linearly on the mass-average residence time in the cell. Therefore, calculation of the residence times at the steady-states before and after a disturbance can be used to predict the response times of the system to a step change in current and flow rate. The effect of blocked flow distributors in one cell in the cell pack was studied for cases when heat transfer was present and absent among the cells. The flow rates showed oscillatory behaviour on blockage of the flow distributors. Presence of heat transfer between the cells dampened the oscillatory behaviour.

Acknowledgement

This work was made possible by financial support from 3M Company.

References

1. J.H. Simons, *in* J. Simons (Ed), 'Fluorine Chemistry' (Academic Press, New York, 1950), p. 414.
2. W.V. Childs, F.W. Klink, J.C. Smeltzer and J.C. Spangler, *US patent 5 322 597*, 21 June (1994).
3. K. Jha, G.L. Bauer and J.W. Weidner, *J Electrochem. Soc.* **145** (1998) 3521.
4. J.A. Drake, J. Newman and C.J. Radke, *J. Electrochem. Soc.* **145** (1998) 1578.
5. S. Prasad, J.W. Weidner and A.E. Farell, *J. Electrochem. Soc.* **142** (1995) 3815.
6. D. Coleman, R.E. White and D.T. Hobbs, *J. Electrochem. Soc.* **142** (1995) 1152.
7. M.M. Saleh, J.W. Weidner, B.E. El-Anadouli and B.G. Ateya, *J. Electrochem. Soc.* **144** (1997) 922.
8. D. Bruggeman, *Ann. Physik*. **24** (1935) 636.
9. M. Ali, M. Sadatomi and M. Kawaji, *Can. J. Chem. Eng.* **71** (1994) 657.
10. G. Wallis, 'One-Dimensional Two-Phase Flow' (McGraw-Hill, New York, 1969).
11. R. Dowlati, M. Kawaji, D. Chisholm and A.M. Chan, *AIChE J.* **38** (1992) 619.
12. N. Clark, R. Flemmer, *AIChE J.* **31** (1985) 500.
13. D. Kern, 'Process Heat Transfer Engineers' Handbook', International edition (McGraw-Hill, New York, 1965).
14. H. Beggs and J. Brill, *J. Petroleum Tech.* (May 1973) 607.